J Mater Sci (2019) 54:3082–3095

Computation

Effect of symmetrical and asymmetrical tilt grain boundaries on the tensile deformation of zirconium bicrystals: a MD-based study

Divya Singh[1], Avinash Parashar[1,*], A. Kedharnath[2], Rajeev Kapoor[2], and Apu Sarkar[2]

[1] *Department of Mechanical and Industrial Engineering, Indian Institute of Technology, Roorkee, India*
[2] *Mechanical Metallurgy Division, Bhabha Atomic Research Center, Mumbai 400085, India*

Received: 23 June 2018
Accepted: 15 October 2018
Published online: 22 October 2018

ABSTRACT

The aim of this article was to study the effect of symmetrical as well as asymmetrical tilt grain boundaries on the tensile deformation of irradiated bicrystalline zirconium. Molecular statics-based simulations were performed to generate both types of tilt grain boundaries with [0001] and $[0\bar{1}10]$ as the tilt axis. Effect of irradiation-induced point defects was studied with respect to deformation mechanism and changes in grain boundary structure of these bicrystals using molecular dynamic simulations. Twinning, formation of dislocation networks and shift in grain boundaries were predicted as the main deformation mechanism. In most of the cases, irradiation-induced defects strain-harden the material. Spatial distribution as well as the number of point defects plays a critical role in the strain hardening of the material subjected to tensile deformation. In grain boundary structures formed with [0001] as the tilt axis, the twinning and dislocation loops formed with irradiation-induced defects govern the deformation mechanism of bicrystalline Zr, whereas in $[0\bar{1}10]$ as the tilt axis, dislocation networks and dislocation density govern the tensile properties in the bicrystals. It can be concluded from the atomistic simulations that structure of grain boundary governs the deformation mechanism of bicrystalline Zr in conjunction with the irradiation-induced defects.

Introduction

During the entire service life, nuclear structures are subjected to extreme irradiation phenomenon [1–4], which introduce many types of geometrical defects such as vacancy, interstitial and dislocation loops [2, 4]. These defects have significant effect on the mechanical and fracture behaviour of nuclear structures [5–9].

Britton et al. [10] studied the deformation mechanism in single crystals and polycrystals of many hcp materials. Their work helps in identifying the conditions that decide the deformation mechanism in hcp crystals. Munroe et al. [11] studied the effect of

Address correspondence to E-mail: drap1fme@iitr.ac.in

https://doi.org/10.1007/s10853-018-3032-7

c/a ratio on the failure modes in hcp Zn crystal. Fan and El-Awady [12] used atomistic modelling technique to study the deformation modes in another hcp material that was magnesium. In another study on hcp materials, researchers performed molecular dynamics (MD)-based simulations to capture the response of tension and compression on the magnesium-based alloys [13]. Liu and Wang [14] have captured grain boundary mobility in magnesium bicrystals subjected to tensile deformation. In a recent work of Tang et al. [15], grain boundary migration in hcp metals was studied with the help of theoretical and atomistic simulations. Geng et al. [16] investigated the presence of ⟨c + a⟩-type sessile dislocation loops in magnesium crystal and held it responsible for high work hardening observed during compression.

In addition to these hcp materials, significant experimental investigations were also performed on the Zr-based alloys [17–19]. Griffith et al. [17] performed experiments in conjunction with dislocation dynamics to study deformation mechanism in Zr–2.5Nb-based alloys. Bailey [19] used electron microscopy to study interaction between dislocations in a deformed crystal of Zr. His experimental studies help in capturing the type and distribution of dislocations emerged in deformed Zr. In addition to these works, researchers have also studied the effect of irradiation on the tensile deformation of Zr. Onchi et al. [20] reported on the basis of their observation that either slip or twinning is the prominent mode of deformation in irradiated samples, depending on the temperature. Rafique et al. [21] performed experiments with polycrystalline Zr to study the effect of irradiation on its tensile deformation.

So far, limited work has been reported on the effects of irradiation on the tensile deformation of bicrystalline Zr. Most of the earlier work on Zr was at the continuum level, which has limitations in capturing the deformation mechanism of bicrystalline Zr. This article will help in elucidating the deformation mechanism of Zr bicrystal as a function of grain boundary structures. In addition, effect of irradiation-induced defects on deformation as well as shift in atomic configuration enforced by irradiation was also studied.

Simulation details

In this article, MD-based simulations were carried out in parallel large-scale atomic/molecular massively parallel simulator (LAMMPS) [22], and post-processing of dump files was performed in OVITO [23]. The reliability and accuracy of any MD-based simulation entirely depend on the type of interatomic potential employed for calculating interatomic interactions. In order to capture the interatomic interactions between Zr atoms, simulations were performed in conjunction with embedded-atom method (EAM) potential parameters proposed by Mendeleev and Ackland [24]. It has been reported in the same article [24] that EAM potential is capable of accurately capturing the mechanical properties of Zr. Moreover, same EAM potential was employed by Divya and Avinash [25] to accurately estimate grain boundary energies as well as point defect formation energies in bicrystalline structure of Zr. Additionally, the same EAM potential was also used by Varvenne and Mackain [26] to study dislocation loop formation in Zr. Zizhe et al. [27] have also employed EAM potential parameters proposed by Mendeleev and Ackland [24] to study the deformation mechanism such as twinning and dislocations in polycrystalline Zr. The prismatic, pyramidal dislocations and twinning, as observed in experiments, are reproduced in their MD simulations. Simulations were carried out to study the effect of irradiation-induced defects on the tensile strength of bicrystals of zirconium. Simulations were performed in three stages. In the first stage, symmetrical tilt grain boundary (STGB) and asymmetrical tilt grain boundary (ATGB) structures were generated in MD-based environment along [0001] and $[0\bar{1}10]$ as the tilt axes. A schematic of the simulation box containing two crystals of Zr along with GB structures is illustrated in Fig. 1.

Two STGB and one ATGB configurations were generated with both the tilt axes. Initially, GB structures along each axis were generated at 0 K. An appropriate deletion criterion was used to delete the overlapping atoms in conjunction with conjugate gradient (CG) algorithm to achieve minimum energy GB configuration. After this, the system is equilibrated to the desired simulation temperature, which was 10 K and 30 K for bicrystals with [0001] and $[0\bar{1}10]$ as the tilt axes, respectively. The equilibration process was carried out for a total time of

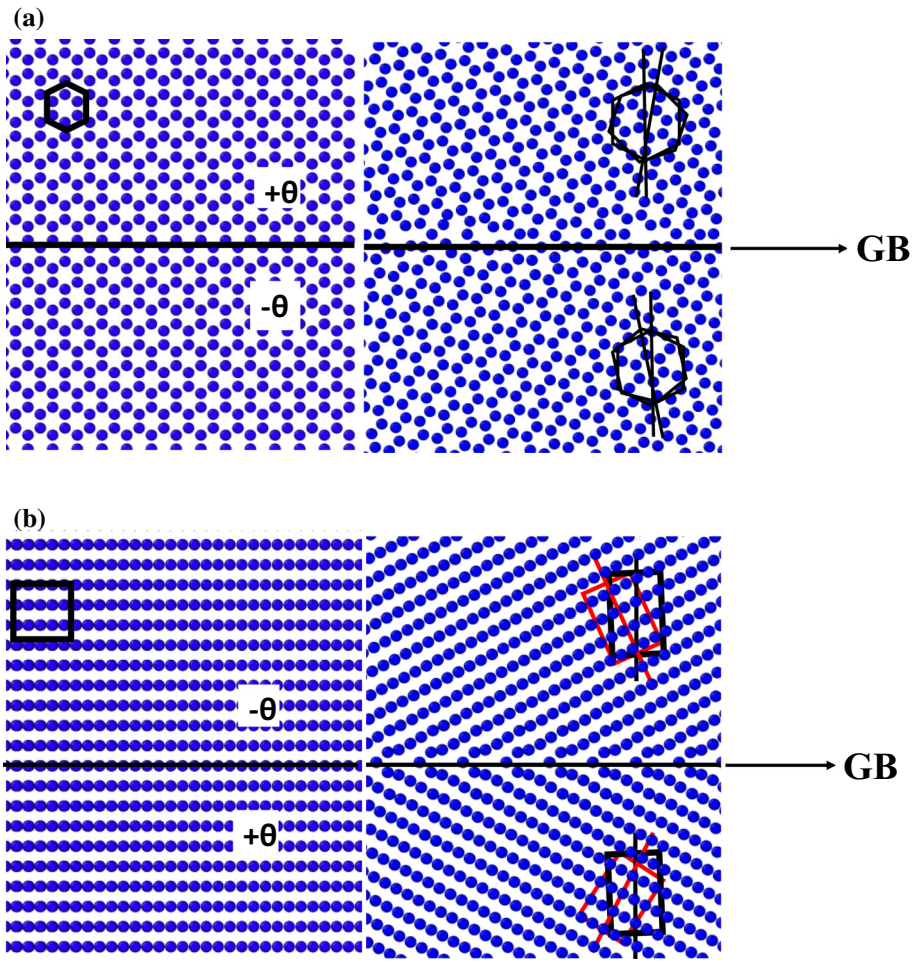

Figure 1 Schematic of the bicrystal of Zr along **a** [0001] tilt axis, **b** [0$\bar{1}$10] tilt axis parameters required to generate STGB and ATGB structures along [0001] and [0$\bar{1}$10] as tilt axes are tabulated in Tables 1 and 2, respectively.

Table 1 Details of the simulations box for STGB and ATGB along [0001] as tilt axis

S. no.	Misorientation angle (2θ)	Inclination angle (Ø)	No. of atoms	Size of simulation box (Å^3)	Nature of the GB structure
1	13.2°	0	218408	130 × 330.8 × 120	Symmetrical
2	44.8	0	251252	145 × 340 × 120	Symmetrical
3	32.3	10°	192625	118 × 320 × 120	Asymmetrical

Table 2 Details of the simulations box for STGB and ATGB along [0$\bar{1}$10] as tilt axis

S. no.	Misorientation angle (2θ)	Inclination angle (Ø)	No. of atoms	Size of simulation box (Å^3)	Nature of the GB structure
1	56.82°	0	328032	112.49 × 340.8 × 200	Symmetrical
2	145.76°	0	224784	115.6 × 227.2 × 200	Symmetrical
3	56.82°	45°	138960	105 × 155 × 200	Asymmetrical

80 picoseconds with a time step of 0.001 picoseconds. All the simulations were performed with periodic boundary conditions imposed in all the principal directions. Further, details about the formation of STGB and ATGB structures were given in our previous work [25]. In the second stage, irradiation-induced defects were generated in the simulation box containing bicrystals of Zr with the help of

displacement cascades. In order to create irradiation-induced defects, e.g. vacancy and interstitials, a primary knock-on atom (PKA) was selected and imparted an energy in the range of 1–2 keV, perpendicular to the grain boundary. The system was relaxed to the desired temperature, which was 10 K and 30 K for [0001] and [0$\bar{1}$10] as the tilt axes, using a Nose–Hoover thermostat. In order to minimise the thermal disturbances, all the simulations were performed at a very low temperature of 10 K or 30 K. Tilt GB structures formed along [0$\bar{1}$10] as the tilt axis were not stable at a low temperature of 10 K; hence, a slightly higher temperature was used in these simulations, but still the temperature in both the cases was kept well below the room temperature. In order to capture the effect of quantity and spatial distribution of these defects, either multiple PKA or PKA positioned at varying distance from GB structures was selected in the simulation box. In the third and final stages, uniaxial tensile loading at a strain rate of 10^9 s^{-1} was applied in the direction aligned perpendicular to the grain boundary plane. During the uniaxial tensile loading, temperature and pressure in the simulation box were maintained with the help of Nose–Hoover thermostat and barostat, with pressure along the transverse direction to loading maintained at zero.

Results and discussion

Separate simulations were performed with the set of grain boundaries generated along [0001] and [0$\bar{1}$10] as the tilt axes. The atomic configuration of STGB and ATGB generated along [0001] as the tilt axis is shown in Fig. 2. Similarly, atomic configurations of the STGB and ATGB generated along [0$\bar{1}$10] as the tilt axis are shown in Fig. 3. In order to capture the atomic configuration of grain boundaries, adaptive common neighbour analysis (a-CNA) was employed with the help of OVITO. In Figs. 2 and 3, red and white colour atoms correspond to perfect hcp structure and dislocation cores, respectively.

It can be inferred from Figs. 2i–ii and 3i–ii that atomic configuration of STGB is more coherent and orderly as compared to corresponding ATGB configurations shown in Figs. 2iii and 3iii, respectively. Isolated dislocation cores in STGB configurations are observed in Fig. 2 containing lower misorientation angles, which more closely resemble the realistic structure reported in the experimental work on polycrystalline Zr [28].

In order to capture the response of tensile loading on the GB structures in conjunction with irradiation-induced defects, single-displacement or multiple displacement cascades were generated at varying distance from the grain boundary plane with PKA energy ranging between 1 and 2 keV. The thermal spike generated in single PKA, as a function of distance from the grain boundary (y = 100 Å, y = 50 Å, y = 5 Å), is demonstrated in Fig. 4. In this article, point defects generated with PKA at a distance of y = 5 Å, 50 Å and 100 Å from the GB are referred as "in GB", "near GB" and "in bulk", respectively.

After generating a stable number of irradiation-induced point defects, the simulation box was subjected to uniaxial tensile loading in a direction perpendicular to the grain boundary plane.

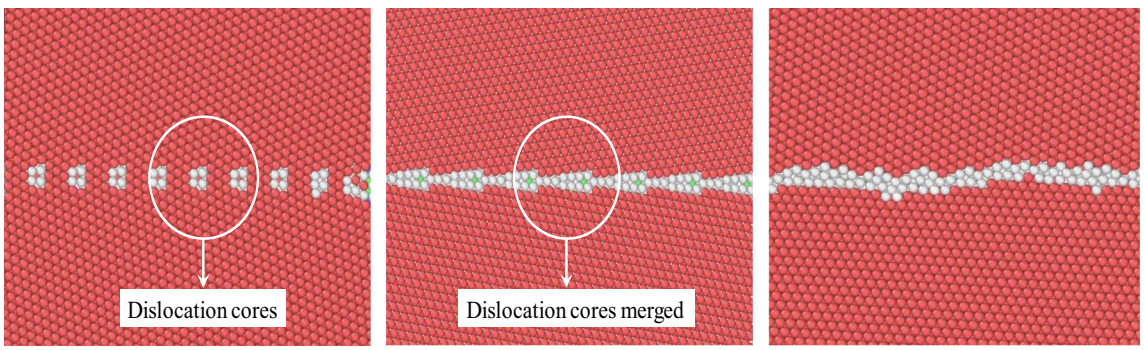

Figure 2 Atomic configuration of grain boundary structure generated along [0001] as the tilt axes with misorientation angle of **i** 13.2° (STGB), **ii** 44.8° (STGB), **iii** misorientation = 32.3° and inclination angle of Ø = 10° (ATGB) (white and red atoms correspond to dislocation cores and Zr atoms in a perfect hcp crystal, respectively).

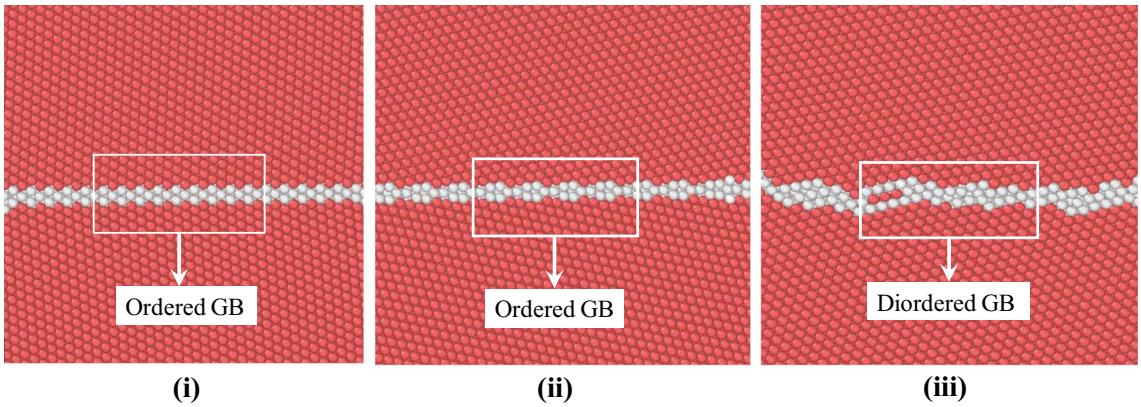

Figure 3 Atomic configuration of grain boundary structure generated along [0$\bar{1}$10] as the tilt axis with misorientation angle of **i** 56.82° (STGB), **ii** 145.76° (STGB), **iii** misorientation = 56.82°, Ø = 45° (ATGB) (white and red atoms correspond to dislocation cores and Zr atoms in a perfect hcp crystal, respectively).

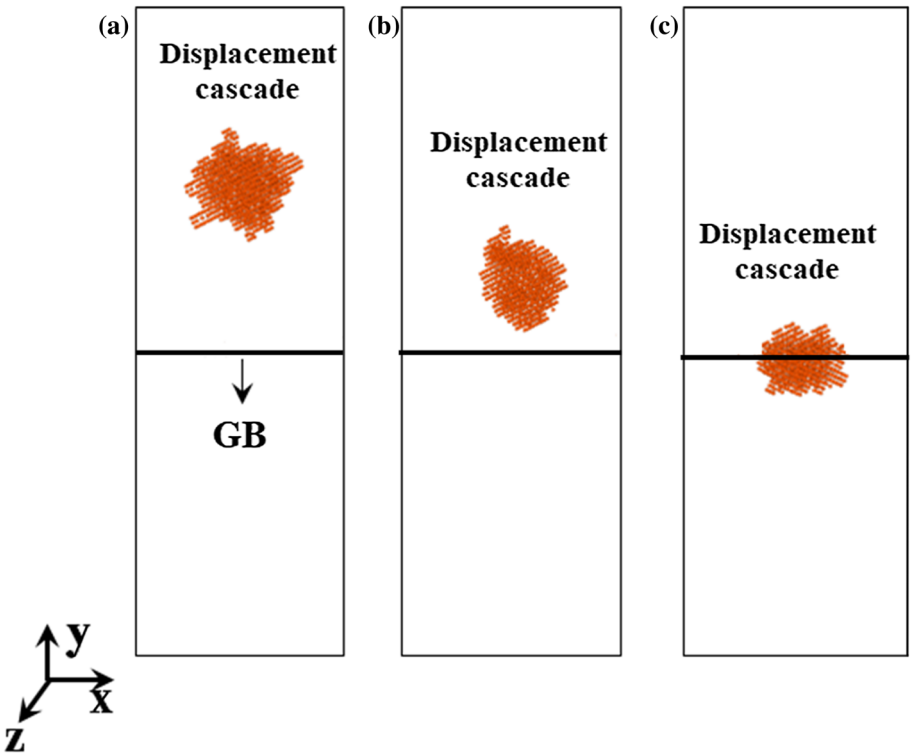

Figure 4 Schematic of thermal spike generated during the displacement cascade as a function of PKA distance from the grain boundary. **a** 100 A (in bulk), **b** 50 Å (near GB), **c** 5 Å (in GB) (orange colour depicts atoms at higher energies, whereas stable atoms are not shown in figure for better clarity).

Bicrystals of Zr formed along [0001] as the tilt axis

Different configurations of irradiation-induced defects were obtained with the help of multiple PKAs and PKA running at varying distance from the GBs, and only results giving maximum variation in the tensile deformation are considered here for further discussion. Stress–strain response for the bicrystal of Zr containing STGB with a misorientation angle of 44.8° is plotted in Fig. 5. In Fig. 5, non-irradiated response is referred as pristine, whereas irradiated bicrystalline structures of Zr were referred with respect to number and position of PKA. It can be observed from the stress–strain response that quantity as well as spatial distribution of irradiation-induced defects has effect on the tensile properties of bicrystalline Zr. It can be inferred from the trend plotted in Fig. 5 that high strength corresponds to simulations performed with higher number of point

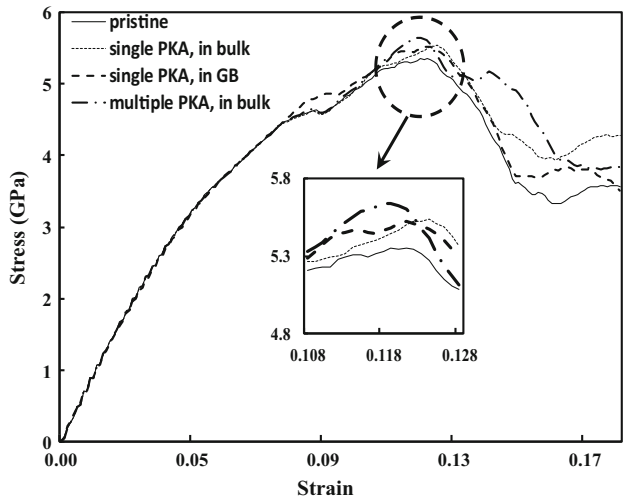

Figure 5 Stress–strain response of STGB with misorientation angle of 44.8° along [0001] as the tilt axis.

defects (multiple cascades). This is in agreement with the theory that the higher the number of point defects, the more will be the chances of interaction with the dislocations and twins. In addition, it is also observed in Fig. 5 that shift in yield or hardening also occurred even with single cascade, that is, lower number of point defects. Thus, not only the number of point defects but also their spatial distribution is critical for inducing strain hardening in bicrystals of Zr. Adaptive common neighbour analysis (a-CNA) was performed with the help of OVITO to analyse the deformation in the atomic configuration of bicrystalline Zr containing a misorientation angle of 44.8°. In order to study the deformation mechanism of the bicrystal of Zr containing a misorientation angle of 44.8°, snapshots of the simulation box were captured at different strain values and are shown in Fig. 6.

It can be observed in Fig. 6 that the primary mode of deformation in simulated bicrystal of Zr containing 44.8° misorientation angle is twinning. Due to the absence of sufficient number of active slip systems in hcp crystals, deformation usually takes via twinning. In Fig. 6, atoms in red and dark green colour correspond to perfect and twinned lattice of a Zr bicrystal. It can also be inferred from Fig. 6 that with the increase in strain, twin dislocations emerging from STGB structure start interacting with the irradiation-induced point defects (encircled in Fig. 6). This interplay between the point defects and emerging twin dislocations induced hardening in irradiated bicrystalline structure of Zr.

In addition to the above-discussed misorientation angle for [0001] as the tilt axis, simulations were also performed with STGB containing a lower misorientation angle of 13.2°. Stress–strain response of non-irradiated (pristine) as well as irradiated bicrystal of Zr is plotted in Fig. 7. As compared to previous bicrystalline structure, lower misorientation angle of 13.2° has shown no hardening in the response plotted in Fig. 7, even with multiple cascades simulated at varying distance from the GB.

At a lower tilt angle, the distribution of dislocations was captured with the help of dislocation extraction algorithm (DXA) and is shown in Fig. 8, which is in agreement with Fig. 2i plotted with the help of a-CNA. Dislocation cores aligned in the STGB plane and separated by the perfect crystal atoms were captured by DXA analysis as depicted in Fig. 8. Straight dislocations with Burger's vector $1/3\langle 1\text{-}210\rangle$ are observed aligned with STGB plane. These predictions are in good agreement with earlier observations made in the experimental work of Bailey [19]. It can be inferred from the trend plotted in Fig. 7 that strain hardening was absent from all the simulations performed either with pristine or irradiated bicrystal of Zr. This is attributed to lower dislocation density, absence of dislocation networks as well as no hindrance to the movement of dislocations, as compared to interaction of twin dislocations with irradiation-induced defects in bicrystal of Zr with higher-angle STGB structures (misorientation = 44.8°). A steep drop in the value of stress is observed in Fig. 7 for irradiated case, after attaining the ultimate stress value, which is attributed to the formation of clear dislocation channels, whereas entanglement of dislocations was observed in simulations performed with pristine bicrystal of Zr as shown in the snapshot of simulation box shown in Fig. 8.

In addition to STGB configurations, simulations were also performed with the ATGB configuration formed along [0001] as the tilt axis. Stress–strain response for the ATGB configuration of bicrystal in conjunction with irradiation-induced defects is plotted in Fig. 9. It can be inferred from the stress–strain response plotted in Fig. 9 that hardening was once again observed in the simulations performed with irradiated ATGB's as compared to pristine.

Deformation of the ATGB at the onset of yield and post-yield is shown in Fig. 10. It can be inferred from Fig. 10 that grain boundary migration and dislocation loops are the dominant modes of deformation in

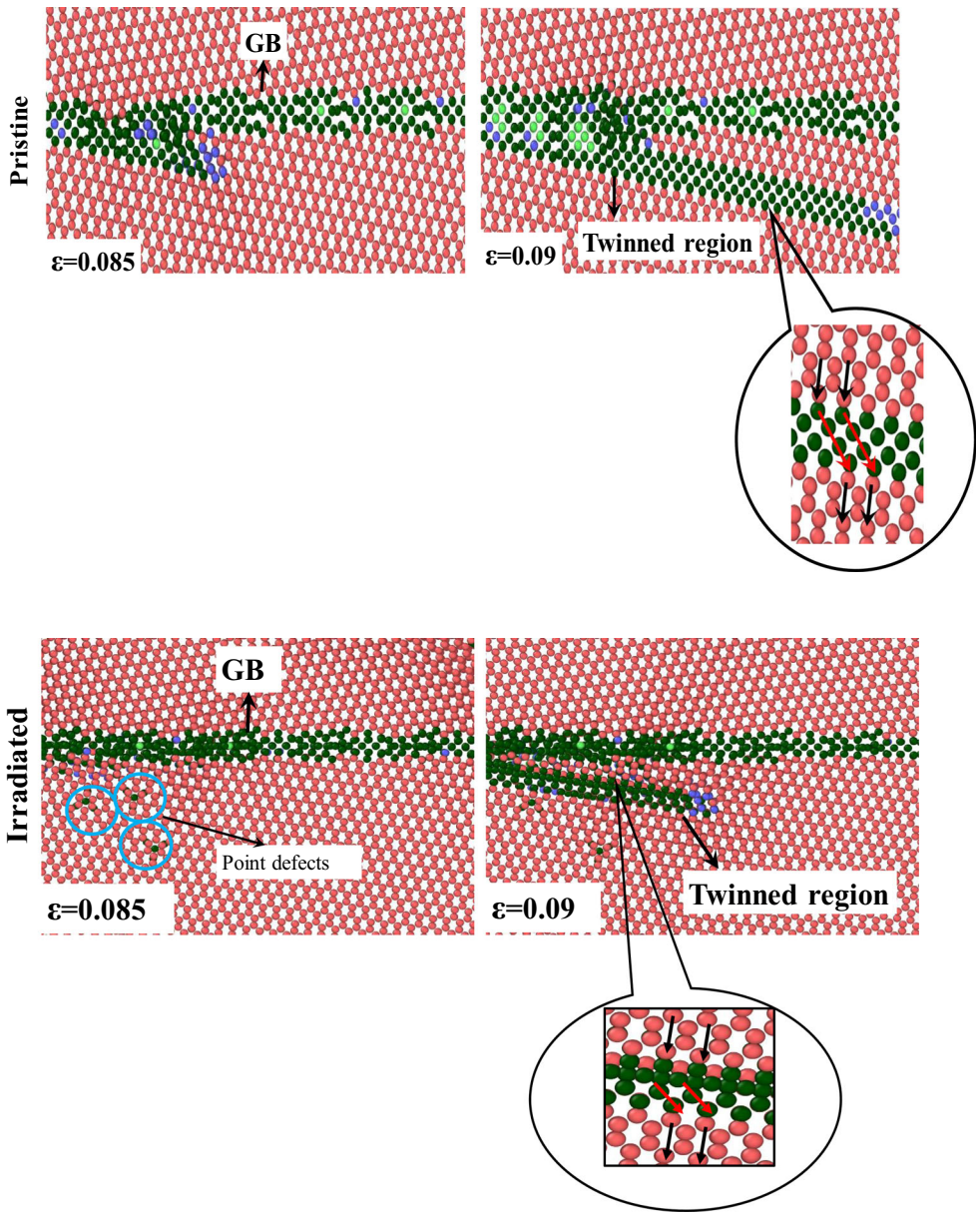

Figure 6 Snapshot of the simulation box at the onset of plasticity in bicrystalline Zr containing STGB with misorientation angle of 44.8° along [0001] as the tilt axis (higher-energy atoms are dark green in colour, whereas irradiation-induced defects are encircled).

pristine and irradiated bicrystals of Zr, respectively. Similar kind of phenomenon was also observed for the hcp bicrystals like Mg and Ti [14, 15].

Grain boundary migration and formation of dislocation loops in the pristine and irradiated bicrystals of Zr were captured in the simulation box with the help of a-CNA and DXA analysis, respectively. The vacancy-type dislocation loop with Burger's vector in the direction $1/3\langle 1\text{-}210\rangle$ formed in irradiated bicrystal of Zr is shown in the snapshot of simulation box shown in Fig. 10. Similar kind of observations was earlier reported in the experimental work of Akhtar and Teghtsoonian [18]. The dislocation loop was only observed in the ATGB configuration simulated in conjunction with the irradiation-induced defects in the close proximity of grain boundaries. Due to the formation of dislocation loops in the irradiated bicrystals of Zr, the strain energy is distributed between ATGB and dislocation loop, which is evident from the movement of dislocation loops in Fig. 10. It can be observed in Fig. 10 that dislocation emerges from ATGB structure in pristine Zr at a strain value

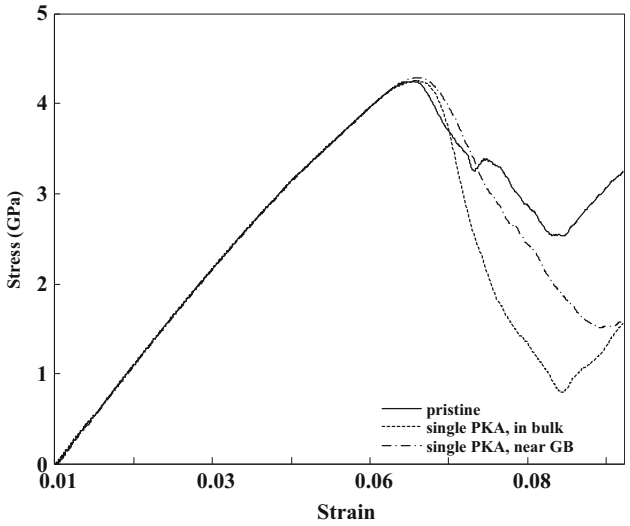

Figure 7 Stress–strain response of STGB with misorientation angle of 13.2° along [0001] as the tilt axis.

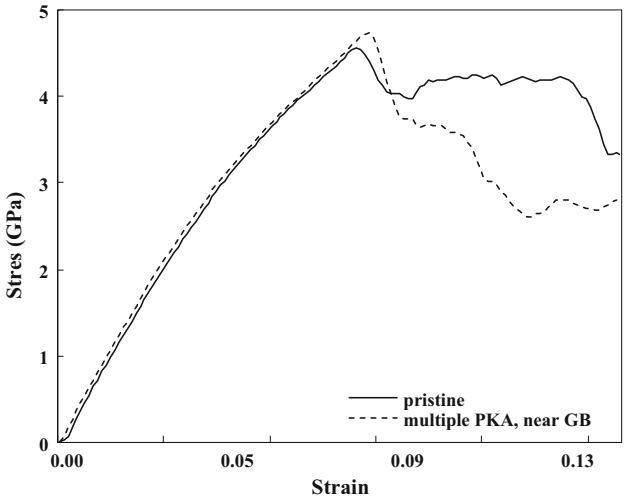

Figure 9 Stress–strain response of ATGB with misorientation = 32.3° and inclination angle (Ø = 10°) along [0001] as the tilt axis.

of 0.078, whereas in irradiated bicrystal, instead of activating dislocations from ATGB, the vacancy defects transform into a dislocation loop in prismatic plane and basal plane. With the increase in strain value to 0.09, the shift in ATGB structure in pristine Zr was evident, whereas the dislocation loop formed in basal plane becomes unstable and moves away in simulation performed with irradiated Zr. This transition in deformation mechanism and redistribution of energy in irradiated bicrystal of Zr is attributed to be the reason behind the strengthening and hardening observed in the stress–strain response.

Bicrystals of Zr formed along $[0\bar{1}10]$ as the tilt axis

A similar procedure, as mentioned in the previous section, was carried out to elucidate the effect of GB structure formed along $[0\bar{1}10]$ as tilt axis on the tensile deformation of bicrystals of zirconium. Stress–strain response for STGB containing a misorientation angle

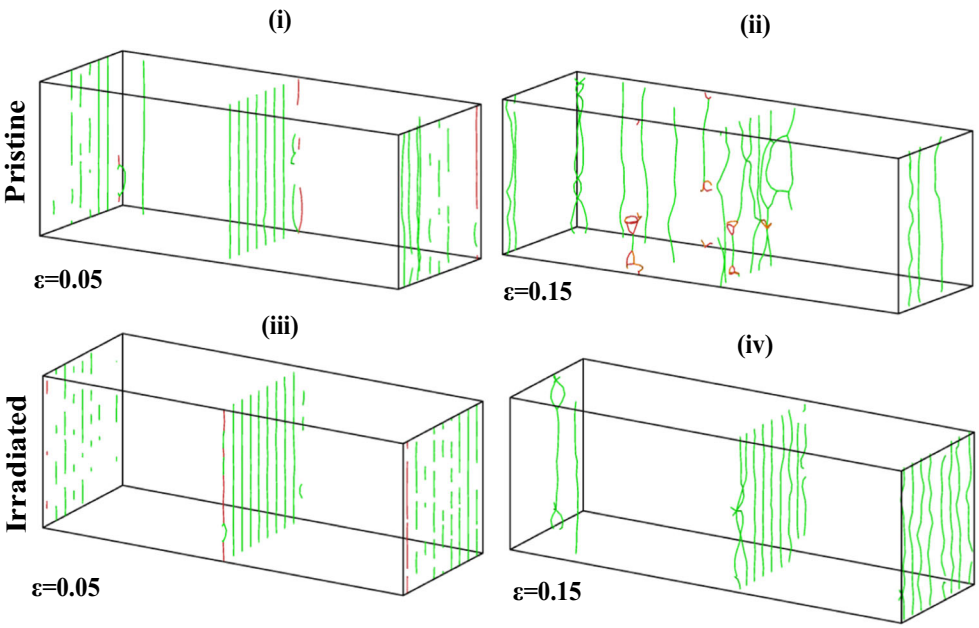

Figure 8 Snapshots of the simulation box at **i** onset of yielding in pristine, **ii** after yield in pristine, **iii** onset of yielding for irradiated, **iv** after yielding in irradiated, STGB bicrystal with misorientation = 13.2° along [0001] as the tilt axis.

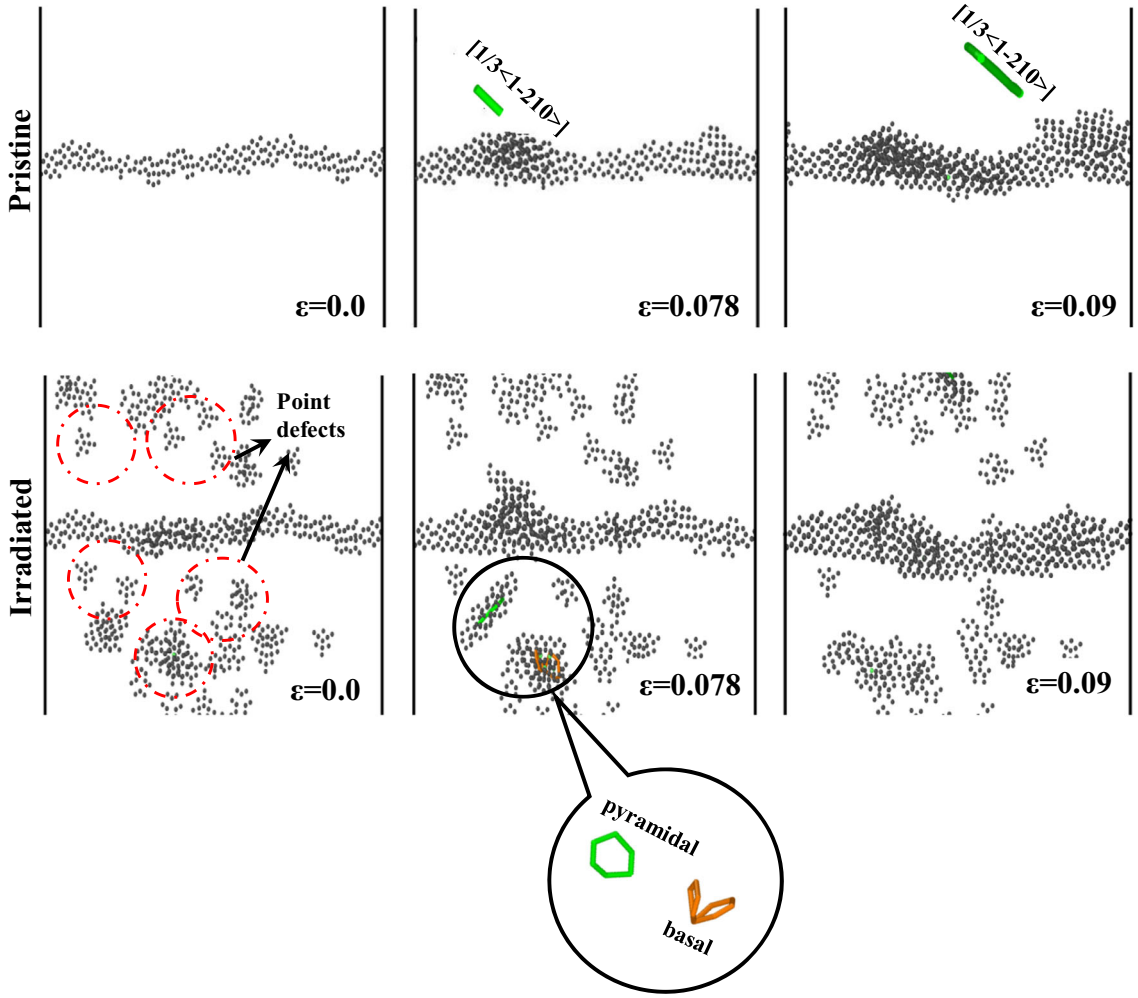

Figure 10 Snapshot of the simulation box containing pristine and irradiated bicrystals of Zr containing ATGB with misorientation and inclination angle of 32.3° and Ø = 10°, respectively, along [0001] as the tilt axis.

of 56.82° is plotted in Fig. 11. It can be inferred from the response plotted in Fig. 11 that hardening was observed in simulations performed with irradiated Zr bicrystals.

In order to capture the deformation mechanism of the bicrystal of Zr, snapshots of the simulation box at the time of onset of yield are shown in Fig. 12. Distinct dislocation networks are observed in the plane of grain boundaries. Similar kind of dislocation networks was quoted in earlier work on Zr [19, 20].

In order to illustrate the phenomenon of hardening in the above-discussed bicrystals of Zr, authors have used the Taylor's hardening expression given in Eq. 1. Hardening or increase in yield strength of a material, as given by Taylor's hardening equation, is proportional to the square root of dislocation density "ρ" [29].

$$\sigma_y = \sigma_o + \alpha M G b \sqrt{\rho}. \quad (1)$$

The difference between σ_y and σ_o helps in predicting any variation or increase in yield strength. Since α, M, G and b are constants in this case, the increase in yield strength is thus directly proportional to the dislocation density (ρ). The dislocation density is calculated as the ratio of total length of dislocations to simulation box volume. Since the simulation cell volume remains same for irradiated and non-irradiated bicrystals with same misorientation, the increase in yield strength can be assumed to be proportional to the square root of dislocation line length. The dislocation line length for each case with the misorientation angle of 56.82° is tabulated in Table 3. Higher dislocation line length promotes a higher ultimate point.

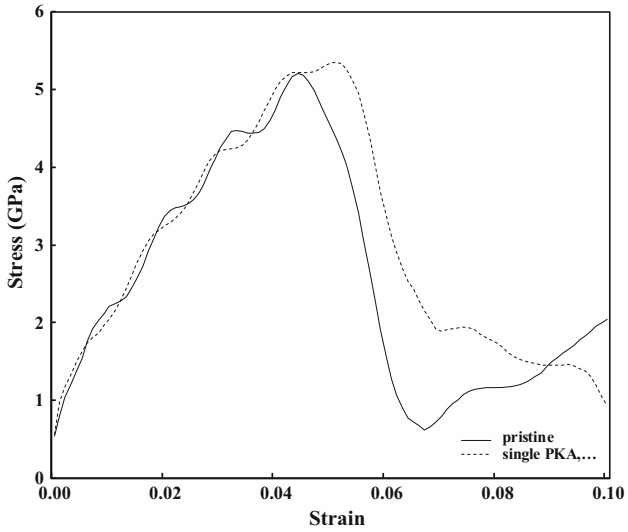

Figure 11 Stress–strain response of STGB with misorientation angle of 56.82° along [0$\bar{1}$10] as the tilt axis.

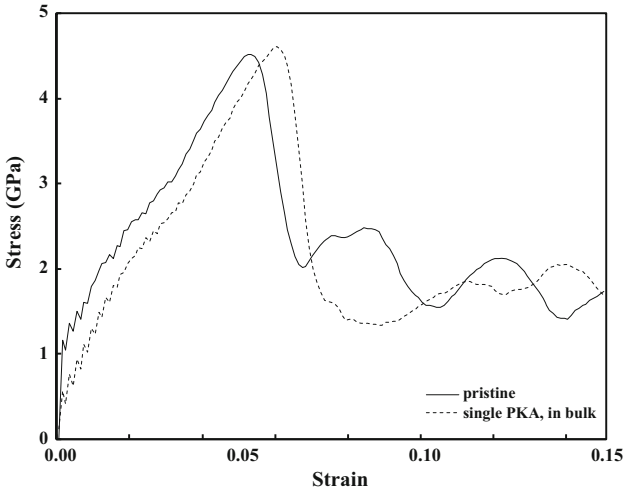

Figure 13 Stress–strain response of STGB with misorientation angle of 145.76° along [0$\bar{1}$10] as the tilt axis.

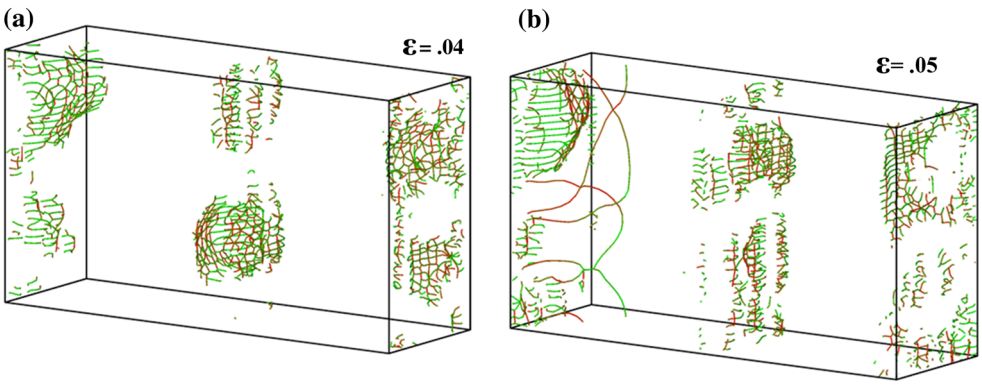

Figure 12 Snapshot of the simulation box containing STGB with misorientation angle of 56.82° along [0$\bar{1}$10] as the tilt axis. **a** Pristine bicrystal, **b** crystal with irradiation-induced defects.

Table 3 Dislocation line length for irradiated and pristine bicrystals

Bicrystal type	Dislocation length (Å) STGB (56.8°)	Dislocation length (Å) STGB (145°)	Dislocation length (Å) ATGB (56.8°)
Pristine	4594.5	376	7737
Irradiated	5608	9238	7663

Similar kind of simulations was performed with STGBs containing misorientation angle of 145° along [0$\bar{1}$10] as the tilt axis. The stress–strain behaviour for these kinds of STGBs is plotted in Fig. 13. Once again, a slight improvement in the yield with irradiation-induced defects is observed in Fig. 13.

Snapshots of the simulation box after DXA analysis are shown in Fig. 14. Prominent dislocation junctions are once again formed in the plane of grain boundary structures. The dislocation junctions dominantly consist of edge-type dislocations in the irradiated bicrystal. The increase in the dislocation networks in the plane of grain boundaries is attributed as the reason behind the strengthening predicted in simulations performed with irradiated bicrystals of Zr. The increase in dislocation density is evident from the data tabulated in Table 3. The dislocation length of pristine form of bicrystals was low at the time of yield, but it jumps to a higher value just after yield, whereas dislocation networks are clearly formed in irradiated bicrystals of Zr.

Similar to [0001] as the tilt axis, ATGB along [0$\bar{1}$10] tilt axis was generated and subjected to tensile loading either in conjunction with irradiation-induced

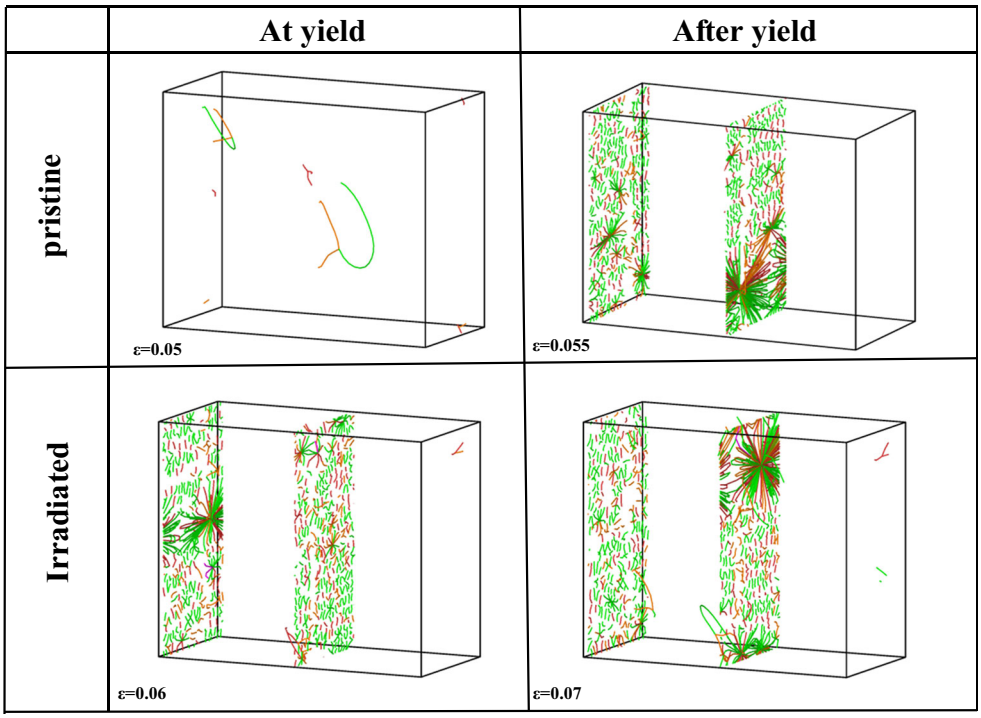

Figure 14 Snapshot of the simulation box containing STGB with misorientation angle of 145.76° along [0$\bar{1}$10] as the tilt axis. Pristine bicrystal, crystal with irradiation-induced defects.

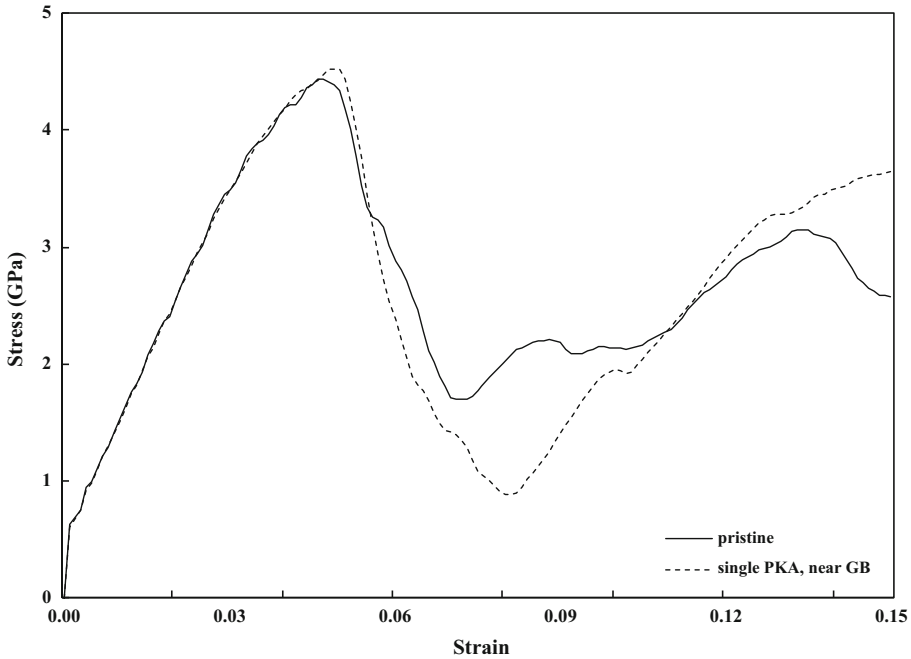

Figure 15 Stress–strain response of ATGB with misorientation angle of 56.82°, inclination angle of Ø = 45° along [0$\bar{1}$10] as the tilt axis.

defects or in pristine form (non-irradiated). Stress–strain response for the ATGB with misorientation and inclination angle of 56.82° and 45°, respectively, is plotted in Fig. 15.

Snapshots of the simulation box at the onset of plasticity are shown in Fig. 16. It can be observed in Fig. 16 that the dislocations emerging from the ATGB structure are equally populated by edge- and screw-type dislocations. In addition to the type of dislocations, a change in the path of movement for dislocation networks was observed in irradiated bicrystal of Zr to interact with the point defects, whereas no such shift was observed in pristine Zr. This interaction between the irradiation-induced defects and

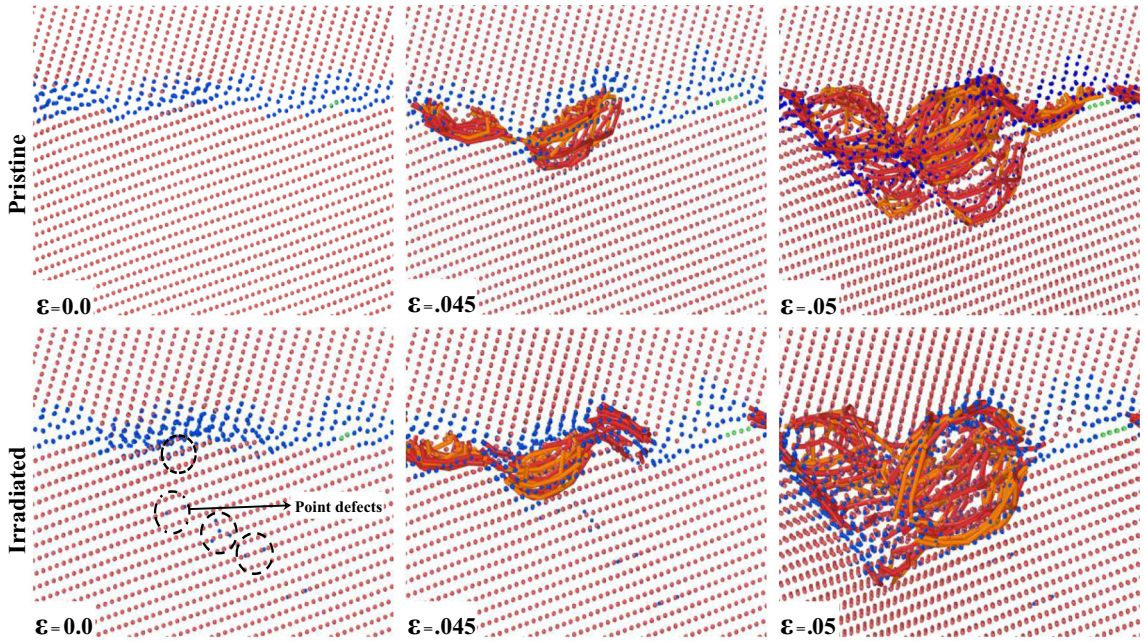

Figure 16 Dislocation generation and evolution under tensile stress in pristine and irradiated bicrystals of Zr (ATGB) at three different sets of strain values corresponding to before yield, at the time of yield and after yield.

Figure 17 Snapshot of the simulation box illustrating the dislocation distributing in STGB and ATGB configuration of bicrystalline Zr without any irradiation-induced defects.

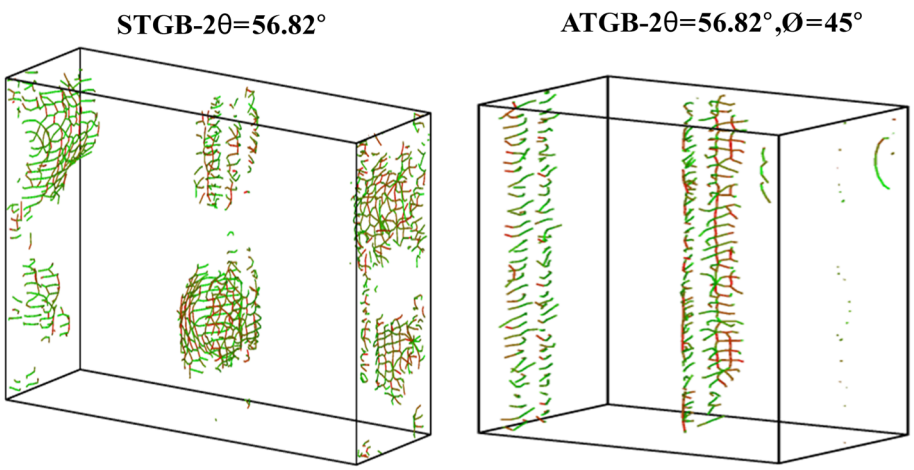

dislocations is attributed to the strengthening observed in stress–strain response in Fig. 15. In ATGB structures, the dominant mode of hardening was the hindrance or interaction of dislocation with the irradiation-induced defects as compared to increase in dislocation density in the previous STGB structures along $[0\bar{1}10]$ as tilt axis (refer Table 3 for dislocation density).

In the end, a comparison between the deformation modes of STGB and ATGB structures containing same misorientation angle of 56.82° is depicted in Fig. 17. It can be concluded that higher strength was observed for STGB structure (Fig. 11), as compared to the corresponding ATGB structure (Fig. 15). In case of STGB, the dislocations are entangled and form closed networks as illustrated in the snapshot of simulation box shown in Fig. 17. This acts like dislocation–dislocation trapping and impedes the movement of dislocation, thus delaying the onset of plasticity. Similar kind of dislocation networks has been attributed to high yield point in a work by Zhang et al. [30]. In case of the ATGB configuration at the same misorientation angle of 56.82°, the dislocations are distinct, small straight lines and rarely form junctions, which can also be observed in Fig. 17.

Conclusion

In this article, MD-based simulations were performed to study the effect of irradiation in conjunction with different types of grain boundaries on the tensile response of zirconium. It can be concluded from the simulations performed with irradiation-induced defects that point defects provide a barrier to the movement of dislocations, hence strain-hardened the zirconium. The degree of strengthening was predicted to be dependent on number of irradiation-induced defects as well as on their spatial distribution.

Two primary modes of deformation—twinning and slip—were observed during uniaxial tensile loading of the Zr bicrystals. Depending upon the tilt axis and misorientation angle, either of the two modes is the prominent mode of failure. Simulations performed with [0001] as the tilt axis predicted twinning and dislocation loops as the prominent mode of deformation, whereas formation of dislocation networks and variation in dislocation density govern the deformation in Zr bicrystal formed along $[0\bar{1}10]$ as the tilt axis.

Acknowledgements

We would like to thank BRNS, Department of Atomic Energy, India (Project No. DAE-984-MID), for providing financial support to this project.

Compliance with ethical standards

Conflict of interest There are no conflicts of interest to declare.

Data availability The raw/processed data required to reproduce these findings cannot be shared at this time as the data also form part of an ongoing study.

References

[1] Chant I, Murty KL (2010) Structural materials issue for the next generation fission reactors. JOM 62:67–74

[2] Parashar A, Singh D (2017) Molecular dynamics based study of an irradiated single crystal of niobium. Comput Mater Sci 131:48–54

[3] Allen T, Busby J, Meyer M, Petti D (2010) Materials challenges for nuclear systems. Mater Today 13:14–23

[4] Rowcliffe AF, Mansur LK, Hoelzer DT, Nanstad RK (2009) Perspectives on radiation effects in nickel-base alloys for applications in advanced reactors. J Nucl Mater 392:341–352

[5] Holt RA, Gilbert RW (1986) <c > Component dislocations in annealed Zircaloy irradiated at about 570 K. J Nucl Mater 137:185–189

[6] Holt RA (1988) Mechanisms of irradiation growth of alpha-zirconium alloys. J Nucl Mater 159:310–338

[7] Fainstein-Pedraza D, Savino EJ, Pedraza AJ (1978) Irradiation-growth of zirconium-base alloys: part I. J Nucl Mater 73:151–168

[8] Charit I, Murty KL (2008) Creep behavior of niobium-modified zirconium alloys. J Nucl Mater 374:354–363

[9] Shishov VN, Peregud MM, Nikulina AV, Kobylyansky GP, Novoselov AE, Ostrovsky ZE et al (2005) Influence of structure d phase state of Nb containing Zr alloys on irradiation-induced growth. J ASTM Int 2:666–685

[10] Britton TB, Dunne FPE, Wilkinson AJ (2015) On the mechanistic basis of deformation at the microscale in hexagonal close-packed metals. Proc R Soc A 471:20140881

[11] Munroe N, Tan X (1997) Orientation dependence of slip and twinning in HCP metals. Scr Mater 36(12):1383–1386

[12] Fan H, El-Awady JA (2015) Molecular dynamics simulations of orientation effects during tension, compression and bending deformations of magnesium nanocrystals. J Appl Mech 82:1–101006

[13] Mahata A, Sikdar K (2016) Molecular dynamics simulation of nanometer scale mechanical of hexagonal Mg–Li alloy. J Magnes Alloys 4:36–43

[14] Liu X, Wang J (2016) Low-energy, mobile grain boundaries in magnesium. Sci Rep 6:21393. https://doi.org/10.1038/srep21393

[15] Tang S, Zhang G, Zhou N, Guo TF, Huang XX (2017) Uniaxial stress-driven boundary migration in hexagonal close-packed (HCP) metals: theory and simulations. Int J Plast 95:82–104. https://doi.org/10.1016/j.ijplas.2017.04.001

[16] Geng J, Chisholm MF, Mishra RK, Kumar KS (2014) The structure of $\langle c + a \rangle$ type dislocation loops in magnesium. Philos Mag Lett 94(6):377–386

[17] Griffiths M, Sage D, Holt RA, Tome CN (2002) Determination densities in HCP metals from X-ray diffraction line-broadening analysis. Metall Mater Trans A 33A:859–865

[18] Akhtar A, Teghtsoonian A (1971) Plastic deformation of zirconium single crystals. Acta Metall 19:655–663

[19] Bailey JE (1962) Electron microscope studies of dislocations in deformed zirconium. J Nucl Mater 7(3):300–310

[20] Onchi T (1977) Effect of neutron irradiation on deformation behaviour of zirconium. J Nucl Sci Technol 14(5):359–369

[21] Rafiqe M, Afzal N, Ahmad R, Ahmad S, Ghauri IM (2012) Mechanical behaviour of low-dose neutron-irradiated polycrystalline zirconium. Radiat Effects Defects Solids 167(4):289–297

[22] Plimpton S (1995) Fast parallel algorithms for short range molecular dynamics. J Comput Phys 117:1–19

[23] Stukowski A (2010) Visualization and analysis of atomistic simulation data with OVITO-the open visualization tool. Model Simul Mater Sci Eng 18:015012

[24] Medelev MI, Ackland GJ (2007) Development of an interatomic potential for the simulation of phase transformations in zirconium. Philos Mag Lett 87(5):349–359

[25] Singh D, Parashar A (2018) Effect of symmetrical and asymmetrical tilt grain boundaries on radiation induced defects in zirconium. J Phys D Appl Phys 51(2018):265301

[26] Varvenne C, Mackain O, Clouet E (2014) Vacancy clustering in zirconium: an atomic-scale study. Acta Mater 78:65–77

[27] Zizhe Lu, Noordhoek MJ, Chernatynskiy Aleksandr, Sinnott SB, Phillpot SR (2015) Deformation processes in polycrystalline Zr by molecular dynamics simulations. J Nucl Mater 462:147–159

[28] Wang Y, Li J, Ye H (1996) Structure analysis of the Z = 7 ((1230)/[0001] 21.8°) grain boundary in α-Ti. Philos Mag A 73(1):213–222

[29] Singh D, Parashar A (2018) Effect of symmetric and asymmetric tilt grain boundaries on the tensile behaviour of bcc-niobium. Comput Mater Sci 143:126–132

[30] Hui Zhang X, Wang Peng Wang, Zhan Xun, Zhou Yanchun (2015) Insights into high-temperature uniaxial compression deformation behaviour of Ti_3AlC_2. J Am Ceram Soc 98(10):3332–3337